



### **Science Arts & Métiers (SAM)**

is an open access repository that collects the work of Arts et Métiers Institute of Technology researchers and makes it freely available over the web where possible.

This is an author-deposited version published in: <https://sam.ensam.eu>  
Handle ID: <http://hdl.handle.net/10985/17265>

#### **To cite this version :**

Thierry PALIN-LUC, Pierre OSMOND, Michel BLANC, Charles BRUGGER - Gigacycle fatigue behavior of a cast aluminum alloy under biaxial bending: experiments with a new piezoelectric fatigue testing device - Procedia Structural Integrity p.1173-1180 - 2016

Any correspondence concerning this service should be sent to the repository

Administrator : [scienceouverte@ensam.eu](mailto:scienceouverte@ensam.eu)





21st European Conference on Fracture, ECF21, 20-24 June 2016, Catania, Italy

# Gigacycle fatigue behavior of a cast aluminum alloy under biaxial bending: experiments with a new piezoelectric fatigue testing device

Charles Brugger<sup>a,\*</sup>, Thierry Palin-Luc<sup>a</sup>, Pierre Osmond<sup>b</sup>, Michel Blanc<sup>b</sup>

*To Claude Bathias memory*

<sup>a</sup>Arts et Metiers ParisTech, I2M, CNRS, Esplanade des Arts et Métiers, 33405 Talence, France

<sup>b</sup>PSA Peugeot Citroën, 18 rue des fauvelles, 92256 La Garenne-Colombes cedex

---

## Abstract

A new ultrasonic fatigue testing device has been developed to test specimens under biaxial loading at 20 kHz. A flat smooth specimen with a disc geometry is placed on a circumferential frame and cyclically loaded at the center of its upper face. Disc bending generates a biaxial proportional stress state at the center of the lower face. Any positive loading ratio can be applied. A cast aluminum alloy (used to produce cylinder heads) has been tested under biaxial loading using this device in order to determine its fatigue strength at  $10^9$  cycles under high hydrostatic pressure. Self-heating is moderate but macroscopic fatigue cracks after testing are very long. First results in VHCF regime are consistent with literature results obtained under similar stress state for the same material, but in HCF regime and at 20 Hz.

Copyright © 2016 The Authors. Published by Elsevier B.V. This is an open access article under the CC BY-NC-ND license (<http://creativecommons.org/licenses/by-nc-nd/4.0/>).

Peer-review under responsibility of the Scientific Committee of ECF21.

*Keywords:* Gigacycle fatigue, biaxial loading, bending, cast aluminum alloy, ultrasonic testing machine

---

## 1. Introduction

Many components in several industries are loaded in VHCF regime, either at high frequency (wheels of high speed trains, blades in aircraft turbojet engines, etc.) as cited in Bathias and Paris (2005), or at low frequency during

---

\* Corresponding author. Tel.: +33-556845360; fax: +33-556845366.

E-mail address: [charles.brugger@ensam.eu](mailto:charles.brugger@ensam.eu)

decades (artificial heart, mooring chains for off-shore petroleum platforms, etc.) as explained by Palin-Luc et al. (2010). Testing specimens up to  $10^9$  or  $10^{10}$  cycles in a realistic testing time requires to use a very high loading frequency (20 or 30 kHz). Since the work of Mason (1950, 1982) and its first ultrasonic fatigue testing machine under fully reversed tension, several devices using the ultrasonic testing technique have been developed all over the world, especially since the end of the last century. An interesting review is given in Bathias (2006). With such equipment, specimens can be tested under

- tension ( $R=-1$  or  $R>0$  when coupled with electromechanical or servo-hydraulic testing machines)
- torsion ( $R=-1$  or  $R>0$ , by pulse and pause (Stanzl-Tschegg et al. (1993), Mayer (2006)) or continuously (Nikitin et al. (2015))
- 3 points bending ( $R>0$ ) as described by Bathias and Paris (2005)

either in cryogenic environment, at room (with air cooling if needed) or at high temperature (Bathias (2005), Wagner et al. (2012)), in air or in corrosive liquid environment (Perez-Mora et al. (2015)). All these machines allow tests on smooth or notched specimens under uniaxial stress state, but according to our knowledge there is no machine for testing specimens under multiaxial loading.

However, many industrial components are submitted to multiaxial loadings that may lead to a number of cycles close to one billion or more. Fatigue cracks may initiate in areas experiencing multiaxial stress states. That is the reason why a new fatigue testing device has been developed to test specimens under biaxial loading at 20 kHz.

After presenting the principle of a new ultrasonic biaxial fatigue testing device, details are given hereafter on the specimen and machine design, and on the stress state in the specimen. The first results obtained on a cast Al-Si alloy in VHCF regime are then compared with those obtained in literature under similar stress state but in HCF regime and under a lower loading frequency.

## 2. Ultrasonic biaxial fatigue testing device

### 2.1. Principle

The basic principle of an ultrasonic fatigue testing machine is to apply an axial sinusoidal displacement to a specimen at an ultrasonic frequency (typically 20 kHz). The specimen is designed so that it has a natural frequency matching this loading frequency. As partly illustrated in Figure 1b, an ultrasonic fatigue testing machine consists of: (i) a generator applying a 20 kHz sinusoidal electric signal to (ii) a piezoelectric converter that converts the electric signal in a longitudinal vibration at the same frequency, and (iii) a horn (with or without a booster) for amplifying the vibration finally applied to the specimen. The generator is controlled by a computer so that the resonance of the whole system (piezoelectric converter, horn and specimen) is kept all the test long together with the control of the amplitude of the displacement imposed at one end of the specimen.

The new fatigue testing device, presented hereafter (patented in Blanc et al. (2013)), is designed for testing in bending a flat smooth specimen with a disc geometry under ultrasonic frequency. Its principle is similar to the testing apparatus proposed by Koutiri et al. (2011, 2013) but this last one was mounted on a servo-hydraulic testing machine working around 20 Hz only. The specimen is placed on a frame with a torus ring, so that the contact zone between the lower face of the disc and the frame is a circle. A sinusoidal load is applied at the center of the upper face using a hemispherical indenter (Figure 1a). Like in a three points bending test, this leads to the bending of the disc. Using the ultrasonic loading device described in the previous paragraph, a sinusoidal displacement (at 20 kHz) is applied at the center of the specimen. In order to apply a non-zero mean load, this device is coupled to an electromechanical testing machine using 3 columns and hollowed discs attached to the middle of the booster, where there is a vibration node. Since the material remains macroscopically elastic in VHCF regime, any positive loading ratio can be applied. In practice, to be able to carry out a test with uninterrupted contact between specimen and indenter, loading ratios with  $R>0.05$  are recommended.

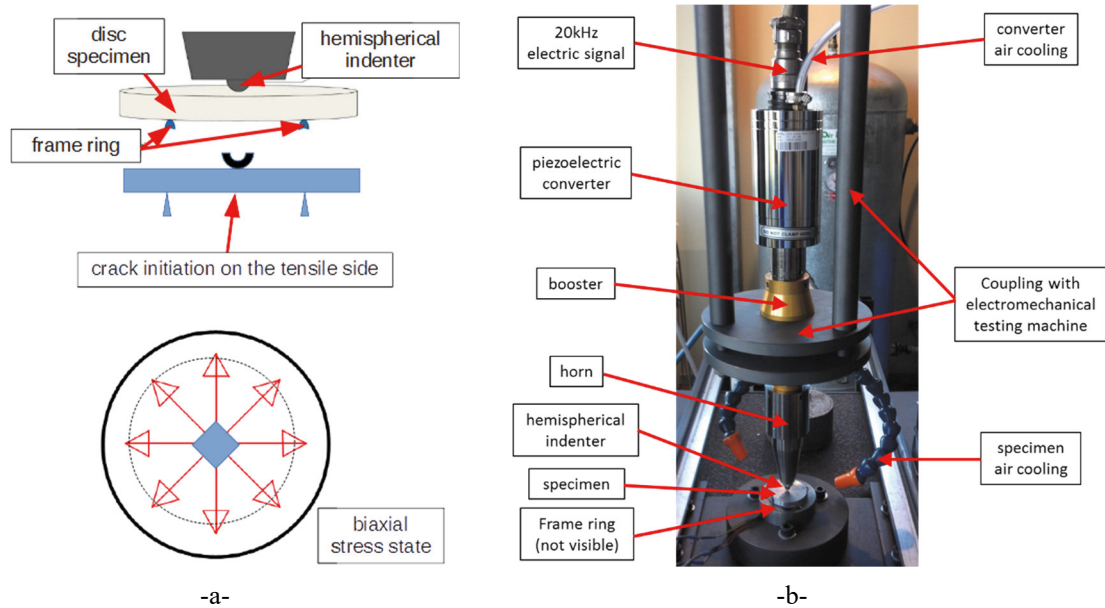


Fig. 1. (a) Principle and (b) Picture of the ultrasonic biaxial fatigue testing device.

## 2.2. Specimen and machine design

As explained in the previous subsection, each part of the machine (booster, horn and specimen) must be carefully designed, so that its natural frequency for axial displacement matches 20 kHz; additionally any other natural modes have to be far from 20 kHz to avoid the risk of parasite vibrations. Critical parts regarding resonance are the specimen and the frame ring. Their geometries were determined by FEA with modal analysis. As explained in Bathias and Paris (2005) for designing tension compression specimens, a preliminary step is the experimental determination of both the density and the dynamic modulus (at 20 kHz) of the tested material using a cylindrical bar.

The specimen tested with the proposed device has a disc geometry (Figure 2b). Its diameter and thickness were determined iteratively using a free-free modal analysis computed with a FEA software. The ideal geometry corresponds to a first natural frequency (associated with biaxial bending) equal to 20 kHz. For the application described in the next section, the thickness has been fixed equal to 6 mm. This is a compromise between the contact forces, which rapidly increase with thickness (for a given stress state at the center of the lower face), and the influence of the local loading on the stress state, which decreases with thickness (the hemispherical indenter is located at the center of the upper face, while the stress state is maximal, in tension, at the center of the lower face where crack will initiate).

In order to minimize the relative displacement between the specimen and the frame (and then the frictional heating), the radius of the frame ring is given by the location of the vibration nodes on the specimen.

## 2.3. Associated stress state on the specimen

Theoretically, disc bending generates an equi-biaxial proportional stress state at the center of the specimen's lower face, and the stress level is proportional to the center's displacement. Tests were performed on three calibration specimens instrumented with strain gauge rosettes glued in the center of the lower face. Different amplitudes of displacement were used, for a static load assuring a positive load ratio. Strains amplitudes were measured using both a wide band conditioning device (Vishay 2210) and high speed data recorder. Since testing conditions are in the VHCF regime, stresses amplitudes were computed assuming an isotropic linear elastic behavior of the material. Results are almost proportional to the displacement. Table 1 summarizes the results on 3 specimens for a given 10  $\mu\text{m}$  amplitude. The stress state can be considered equi-biaxial considering the uncertainties related to

the experimental measurements (location of the strain gauges, gauge factors, etc.). This method was used to determine both static load and sinusoidal displacement levels.

It should be noted that the biaxial stress state is maximal at the center of the lower face. As in a three points bending test, stress amplitudes decrease when moving from the center to the frame ring, or from the surface to the core of the specimen.

Table 1. Stresses at the center of the lower face for a 10 μm amplitude displacement.

| 1 <sup>st</sup> principal stress amplitude (MPa) | 2 <sup>nd</sup> principal stress amplitude (MPa) | Von Mises equivalent stress amplitude (MPa) |
|--|--|---|
| 27.8   | 26.2   | 27.0  |
| 26.9   | 26.6   | 26.8  |
| 28.2   | 26.5   | 27.4  |

### 3. Application to a cast Al-Si alloy

As aforementioned, Koutiri et al. (2009, 2011) proposed a disc bending testing apparatus working around 20 Hz. They investigated the HCF fatigue strength of a cast aluminum alloy used to produce cylinder heads. The new ultrasonic biaxial fatigue testing device has been tested and validated on the same aluminum alloy, so that VHCF results obtained at 20 kHz can be fairly compared to HCF results obtained at 20 Hz. Furthermore, since cylinder heads are submitted to high hydrostatic pressure loadings during a very high number of loading cycles, determining the fatigue strength of this material under similar stress state in the gigacycle regime is useful for a safe very long life fatigue design.

#### 3.1. Material and testing conditions

The material is the cast AlSi7Cu05Mg03 T7. Its conventional yield stress is 250 MPa. Its microstructure has been described by Koutiri (2011) and is displayed in Figure 2a. In order to get microstructure parameters similar to real components (DAS, porosities, hardness, etc.), specimens were machined out of cast cylinder heads. To get enough material volume, cores were diminished prior to casting.

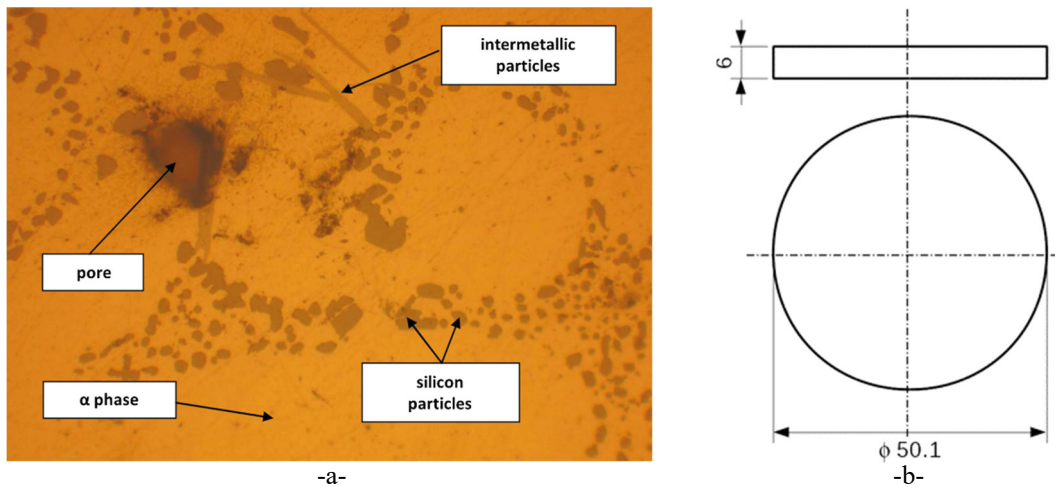


Fig. 2. (a) Microstructure of the AlSi7Cu05Mg03 T7 according to Koutiri (2011) (b) Specimen geometry

The specimen geometry is illustrated in Figure 2b. The frame ring has a 34 mm diameter. Tests are performed in air, at room temperature, with  $R=0.1$  load ratio. Cyclic loading is stopped after  $10^9$  cycles, or when frequency drops down to 19,500 Hz due to fatigue crack initiation and propagation.

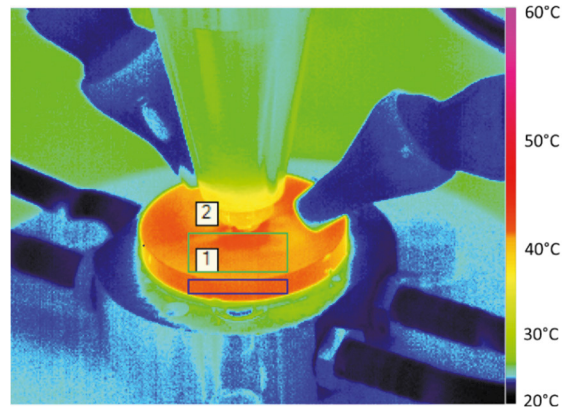


Fig. 3. Temperature measurement by IR camera during ultrasonic fatigue test: areas (1 and 2) used for temperature averaging

Specimen cooling is necessary because ultrasonic loading generates self-heating. Dry compressed air flow is orientated with an air gun towards the upper face (Fig. 1b and 3). In order to quantify self-heating, surface temperature has been measured using an infrared camera FLIR SC 7000 during some selected tests for which the specimen was previously mat black painted for ensuring a high emissivity (Fig. 3). It was not possible to place the camera perpendicular to a surface, because both upper and lower face of the specimen are obstructed (by the ultrasonic loading device and by the frame, Fig. 1b). However, for measuring relative temperature variation compared with initial room temperature, such configuration can be used. Temperature was averaged on the areas labeled 1 and 2 on Figure 3. For maximal stresses equal to 130 – 140 – 150 – 160 MPa, the mean temperature stabilizes respectively at 65 – 75 – 80 – 85°C. Such temperatures are negligible compared to metallurgical transformations of the Al alloy, and to the temperature of a cylinder head under cyclic loading.

### 3.2. Results and discussion

The first fatigue test results are illustrated in Figure 4. The results obtained by Koutiri et al. (2009, 2011) in HCF regime at 20 Hz for the same material and similar stress state are also presented for comparison purpose.

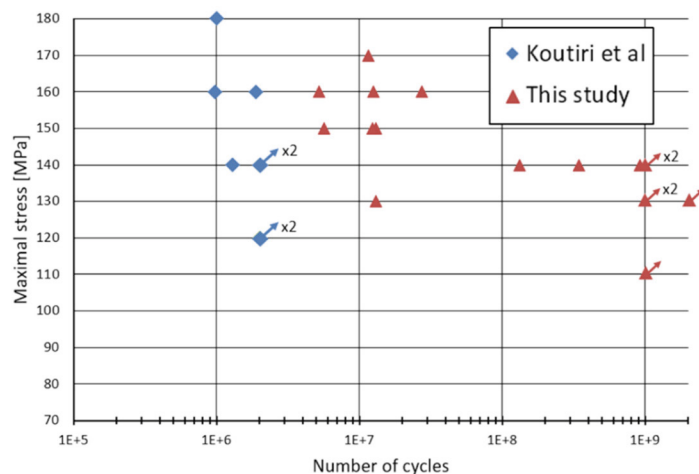


Fig. 4. Fatigue test results under biaxial bending from this study at 20 kHz and from Koutiri et al. (2009, 2011) at 20 Hz on the same material.

For maximum stress levels equal or lower than 140 MPa, the first results obtained with the new ultrasonic biaxial fatigue testing device are in good agreement with the results by Koutiri et al. (2009, 2011). In our data, one specimen broke very early, for a reason to be clarified. Fatigue life also tends to be larger, but we used a hemispherical indenter whereas Koutiri et al. used a ring indenter generating a constant stress state in a 10 mm diameter disk of the lower face. The same tendency would be observed by comparing three points and four points bending tests on a cast material.

The median fatigue strength at  $10^9$  cycles is close to 63 MPa (corresponding to a maximal stress equal to 140 MPa). Figure 5 illustrates, in a Dang-Van diagram, both the experimental median fatigue strengths at  $2 \times 10^6$  cycles obtained by Koutiri (2011) on smooth specimens made in the same cast aluminum alloy, and the threshold line identified from torsion ( $R=-1$ ) and tension ( $R=-1$ ) data. Furthermore, the loading paths corresponding to existing ultrasonic fatigue testing machines are shown: torsion ( $R=-1$ ), tension ( $R=-1$ ), tension or 3 points bending ( $R>0$ ). The loading path corresponding to the specimens tested at the stress level corresponding to  $10^9$  cycles with the new device presented here is illustrated. It is clear that this device allows questioning the Dang-Van criterion for higher hydrostatic stress states. The same conclusion is valid for the Crossland criterion too.

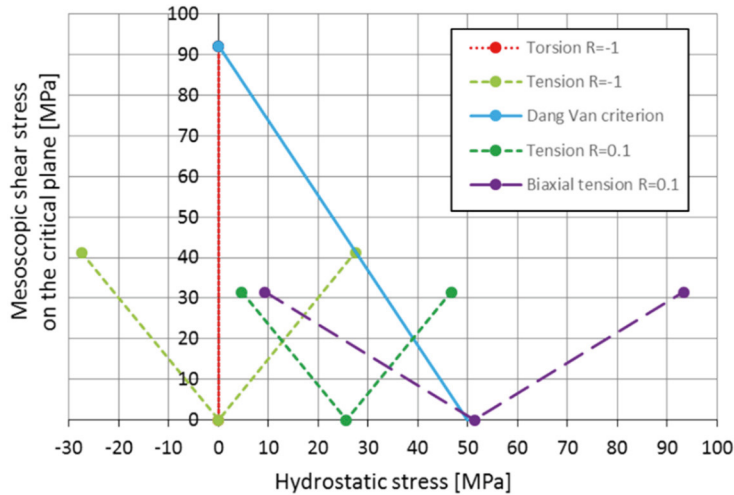


Fig. 5. Macroscopic fatigue crack on the lower face of the specimen a) after testing and b) after breaking it under monotonic quasi-static loading.

For maximum stress levels equal or greater than 150 MPa, another difference between experimental procedures must be accounted for: the stop criterion. Koutiri et al. estimate that the surface length of the macroscopic fatigue cracks is about 6 mm when their tests are interrupted. Our tests were stopped when the resonance frequency decreased from about 19,900 Hz to 19,500 Hz. This frequency drop is due to the rigidity loss associated to the propagation of a very large macroscopic fatigue crack. Indeed, macroscopic cracks are either unique or branched but always extended almost to the radius of the frame ring when the test stops (Fig. 7). Its surface length is thus around 17 mm. Additional investigations are needed to quantify the number of cycles associated with this propagation, but first observations indicate it might exceed  $10^7$  cycles. However, one can note that  $10^7$  cycles represent 1% only of  $10^9$  cycles.

### 3.3. Fractographic analyses

After ultrasonic fatigue testing, the cracked specimens are not broken in two parts (Fig. 6a). For an easy observation of the fatigue crack, each specimen was fractured under quasi-static monotonic loading. To do that, the disc was put on circular ring (like on the ultrasonic testing machine, but with a larger diameter) and a hemispherical indenter put in the center of its upper face and loaded in compression under displacement control by using an electromechanical classic testing machine. When macroscopic fatigue crack is unique (Fig. 6a), quasi-static loading generates two new cracks, and specimen is finally broken in four parts (Fig. 6b).



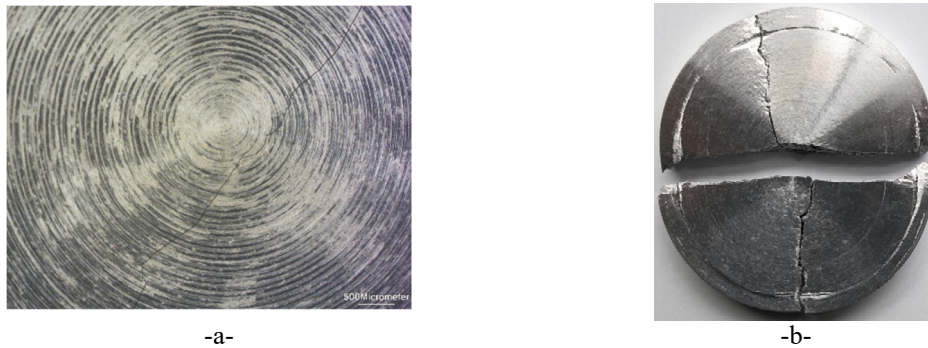


Fig. 6. Macroscopic fatigue crack on the lower face of the specimen a) after testing and b) after breaking it under monotonic quasi-static loading.

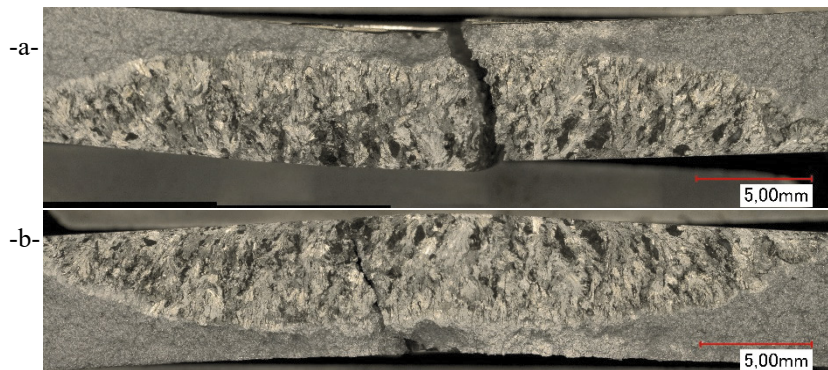


Fig. 7. Macroscopic fatigue crack ( $\sigma_{\max} = 140\text{MPa}$ ;  $N=3.46 \times 10^8$  cyc): a) upper part and b) lower part of the fractured specimen shown in Fig.6b.

Koutiri et al. observed multiple initiation sites on the fracture surfaces of disc specimens tested in bending in HCF regime, unlike specimens tested under uniaxial loading. We made the same observation in VHCF regime: at least 6 initiation sites are visible on the fracture surfaces of the specimen presented in Figure 7. However, we could not determine in which order initiations occurred.

Koutiri et al. also showed that the tested cast aluminum alloy contains relatively small ( $\sim 100\ \mu\text{m}$ ) casting defects (shrinkages, pores), and that most of fatigue cracks initiate on these casting defects. Indeed, such defects are responsible for fatigue crack initiation both in HCF and in VHCF regime. This can be seen in Figure 8 where two fatigue crack initiations are very close to shrinkages with sizes close to  $100\ \mu\text{m}$ .

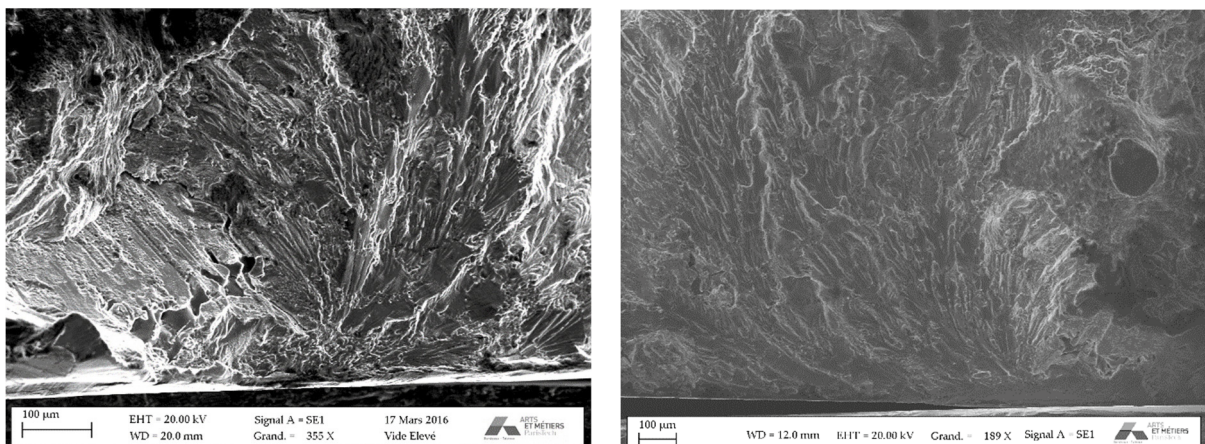


Fig. 8. Two fatigue crack initiations close to shrinkages ( $\sigma_{\max} = 160\text{MPa}$ ;  $N=2.7 \times 10^8$  cyc).



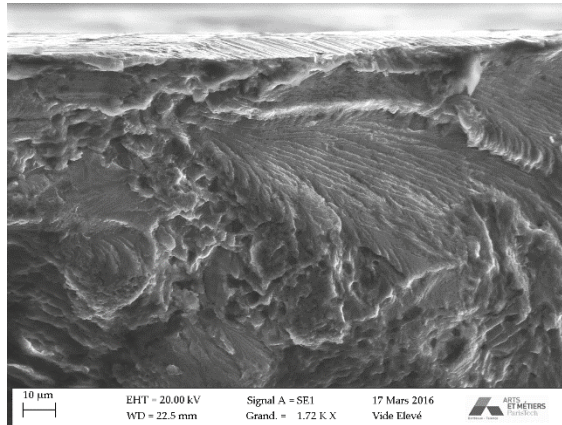


Fig. 9. Fatigue crack initiation between alpha phase and eutectic silicon particles ( $\sigma_{\max} = 140\text{MPa}$ ;  $N=1.3 \times 10^8$  cyc).

Finally, Koutiri et al. also observed some crack initiations on silicon or intermetallic particles. Figure 9 illustrates a crack initiation that occurred between the alpha phase and silicon particles (without any casting defect).

#### 4. Conclusion and prospects

A new ultrasonic fatigue testing device generating a biaxial proportional stress state in the critical area of the specimen with a positive loading ratio has been designed and tested. For validating this equipment, VHCF tests were performed on a cast aluminum alloy already tested in the literature in HCF regime under a similar stress state. The new results are consistent with data from the literature. Self-heating is moderate, but the stop criterion could be improved to detect smaller crack. Fracture mechanisms are also consistent with the literature for the tested cast aluminum alloy: multiple crack initiations occurred, either on casting defects (pores or shrinkages), or between alpha phase and silicon particles. Additional work has to be done to identify the crack initiation area.

#### References

- Bathias, C., Paris, P.C., 2005. Gigacycle Fatigue in Mechanical Practice. Marcel Dekker, New York.
- Bathias, C., 2006. Piezoelectric fatigue testing machines and devices. *International Journal of Fatigue* 28, 1438–1445.
- Blanc, M., Osmond, P., Palin-Luc, T., Bathias, C., 2013. French patent N° FR1357198.
- Koutiri, I., Morel, F., Bellett, D., Augustins, L., 2009. Effect of high hydrostatic stress on the fatigue behavior of metallic materials. 12<sup>th</sup> International Conference on Fatigue, Ottawa.
- Koutiri, I., 2011. Effet des fortes contraintes hydrostatiques sur la tenue en fatigue des matériaux métalliques, PhD thesis, ENSAM, N° 2011-ENAM-0015.
- Koutiri, I., Bellett, D., Morel, F., Augustins, L., Adrien, J., 2013. High cycle fatigue damage mechanisms in cast aluminium subject to complex loads. *International Journal of Fatigue* 47, pp. 44–57.
- Mason, W.P., 1950. Piezoelectric Crystals and their application in ultrasonics. Van Nostrand, New York, pp. 161.
- Mason W.P., 1982. Ultrasonic fatigue: Proceedings of the First International Conference on Fatigue and Corrosion Fatigue Up to Ultrasonic Frequencies. Well, J.M., Buck Roth, O.L.D., Tien, J.K. (Ed.). The Metallurgical Society of AIME, (PA) USA, pp. 87–102.
- Mayer, H., 2006. Ultrasonic torsion and tension–compression fatigue testing: Measuring principles and investigations on 2024-T351 aluminium alloy. *International Journal of Fatigue* 28, pp. 1446–1455.
- Nikitin, A., Bathias, C., Palin-Luc, T., 2015. A new piezoelectric fatigue testing machine in pure torsion for ultrasonic gigacycle fatigue tests: application to forged and extruded titanium alloys. *Fatigue and Fracture of Engineering. Materials and Structures* 38, pp. 1294–1304.
- Palin-Luc, T., Perez-Mora, R., Bathias, C., Dominguez, G., Paris, P.C., Arana, J-L, 2010. Fatigue crack initiation and growth on a steel in the very high cycle regime with sea water corrosion. *Engineering Fracture Mechanics* 77, pp. 1953–1962.
- Perez-Mora, R., Palin-Luc, T., Bathias, C., Paris, P.C., 2015. Very high cycle fatigue of a high strength steel under sea water corrosion: A strong corrosion and mechanical damage coupling. *International Journal of Fatigue* 74, 156–165.
- Stanzl-Tschegg, S.E., Mayer, H. R., Tschegg, E. K., 1993. High frequency method for torsion fatigue testing. *Ultrasonics* 31, pp. 275–280.
- Wagner, D., Cavalieri, F.J., Bathias, C., Ranc, N., 2012. Ultrasonic fatigue tests at high temperature on an austenitic steel. *Propulsion Power Research* 1, pp. 29–35.